# ESI-MS Studies and Calculations on Second-Generation Grubbs and Hoveyda–Grubbs Ruthenium Olefin Metathesis Catalysts

Hao-Yang Wang,[†] Wai-Leung Yim,[‡] Yin-Long Guo,[†] and Jürgen O. Metzger*,[§]

[†]Shanghai Mass Spectrometry Center, Shanghai Institute of Organic Chemistry, Chinese Academy of Sciences, Lingling Road 345, 200032 Shanghai, People's Republic of China

[‡]Institute of High Performance Computing, 1 Fusionopolis Way, #16-16 Connexis, Singapore 138632, Singapore

[§]Institut für Reine und Angewandte Chemie, Carl von Ossietzky Universität Oldenburg, Carl-von-Ossietzky-Straße 9-11, 26129 Oldenburg, Germany.

Ⓢ *Supporting Information*

ABSTRACT: Electrospray ionization mass spectrometry (ESI-MS) and subsequent MS/MS methods were used to study second-generation Grubbs catalysts **2** and **3** and first- and second-generation Hoveyda–Grubbs catalysts **4** and **5**, respectively, as well as the pyridine-tethered Ru carbene catalyst **6**. Direct ESI-MS analyses of Ru catalysts **2**–**6** showed the corresponding radical cations $2^{•+}$–$6^{•+}$ and the protonated ligand PCy_3 and H_2IMes, respectively. Alkali metal adduct ions $2 \cdot M^+$ and $3 \cdot M^+$ (M = Li, Na, K, Cs) and $4 \cdot M^+$–$6 \cdot M^+$ (M = Li, K) could be easily obtained by mixing the CH_2Cl_2 solution of catalysts **2**–**6** with the CH_3OH solution of alkali-metal chloride using an online microreactor coupled directly to the electrospray ion source of a quadrupole time-of-flight (Q-TOF) mass spectrometer and were studied by collision-induced dissociation (CID). Remarkably, the alkali metal cationized 14-electron Ru complexes $2a \cdot M^+$ and $3a \cdot M^+$ formed by dissociation of phosphine from **2** and **3**, respectively, were detected directly from solution. The ratio $[2a \cdot M^+]/[2 \cdot M^+]$ increased with decreasing Lewis acidity of M^+ from Li^+ to Cs^+. Moreover, theoretical computations were performed on Ru complexes **2**, **5**, and **6**, showing good agreement with experimental X-ray diffraction data and providing more structural information about the alkali metal adduct ions $2 \cdot M^+$, $5 \cdot M^+$, and $6 \cdot M^+$ (M = Li, K) as well as about the 14-electron species **2a**, **5a**, and **6a** and the respective alkali metal adduct ions.
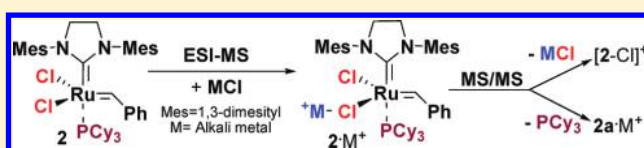
INTRODUCTION

Mass spectrometric ionization methods at atmospheric pressure (API) such as electrospray ionization (ESI)[1,2] allow the measurement and characterization of metal–organic complexes and catalysts directly from solution.[3] ESI-MS was also applied to investigate reactive intermediates from solution of reactions catalyzed by various catalysts,[4,5] providing new insights into the mechanism of the reactions studied, including some important homogeneously catalyzed reactions.[6,7] Ruthenium carbene based olefin metathesis is a powerful reaction in organic and polymer synthesis.[8,9] It is of great interest to be able to study the ESI-MS behavior of the neutral Ru carbene metathesis catalysts[10] and to investigate the ongoing metathesis reactions in solution. Recently, we reported on the online ESI-MS studies of first-generation Grubbs catalysts, such as $(PCy_3)_2Cl_2Ru=C(H)Ph$ (**1**), and some metathesis reactions in solution using the in situ exchange of a neutral phosphine ligand against a "charge-labeled" phosphine[11] and, more advantageously, the in situ alkali metal cationization strategy.[12] We were able to characterize mass spectrometrically two first-generation ruthenium catalysts and reactive Ru intermediates in the catalytic cycle of some important metathesis reactions, including ring-closing metathesis (RCM), acyclic diene metathesis (ADMET), and ring-opening metathesis polymerization (ROMP).[12] Moreover, we could show that the catalytic activity was reduced with increasing Lewis acidity of the alkali metal cation but not
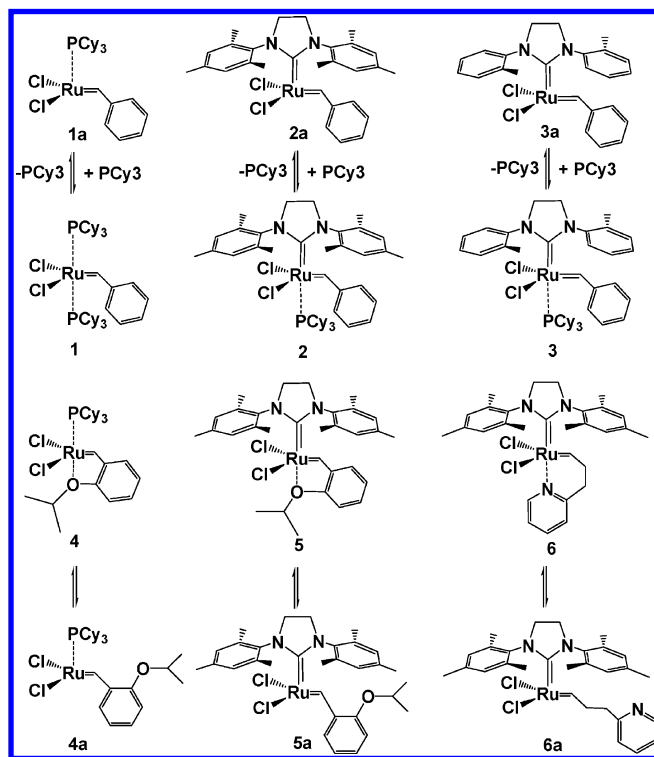
suppressed. Second-generation Grubbs[13] and Hoveyda–Grubbs Ru catalysts[14] are more widely used due to their higher activity and lower decomposition rate, as well as their tolerance to different functional groups and higher temperature in comparison to first-generation catalysts.

In this article, we report on ESI-MS studies of the second-generation Grubbs catalysts **2** and **3**[13] and the Hoveyda–Grubbs catalysts **4** and **5**[14] as well as the pyridine-tethered catalyst **6**[15] (Scheme 1) and the feasibility of alkali metal cationization strategy[12] to study mass spectrometrically these important catalysts. We also investigated the gas-phase fragmentation behaviors of the formed ionic species by ESI tandem mass spectrometry (ESI-MS/MS). Moreover, theoretical computations were performed to provide more structural and energetic information for the alkali metal adduct ions of the catalysts **2**, **5**, and **6**. We compare our computational results with experimental X-ray diffraction data and with previous computations,[16] as well as with our computational results for the alkali metal adduct ions of the first-generation Grubbs catalyst **1**.[12]

Scheme 1. Ruthenium Olefin Metathesis Catalysts 1−6 and the Respective Catalytically Active 14-Electron Complexes 1a−6a

of theory, and for Ru a Los Alamos National Laboratory 2-double-ζ (LANL2DZ) basis set with effective core potential was adopted.[17]

■ RESULTS

1. Direct ESI-MS Study of Ru Catalysts 2−6. As the starting point, we studied the ESI mass spectrometric behavior of catalysts **2−6**. Catalyst **2** in CH_2Cl_2 solution showed clearly the corresponding radical cation $\mathbf{2}^{\bullet+}$ at m/z 848 (Figure 1a),
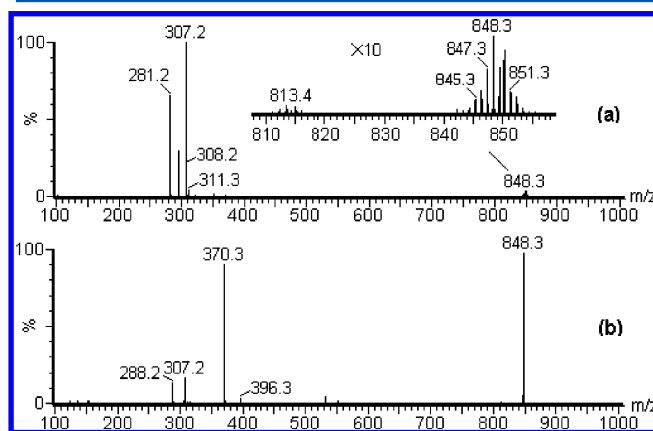
Figure 1. (a) ESI mass spectrum of Ru catalyst **2** dissolved in CH_2Cl_2 and (b) ESI-MS/MS spectrum for CID of $\mathbf{2}^{\bullet+}$ at m/z 848.

which was comparable to first-generation Ru catalyst **1**.[11] We also observed some heterolysis of complex **2** to give the low-abundance cation $[\mathbf{2} - Cl]^+$ at m/z 813 (see insert Figure 1a). Interestingly, the base peak of the ESI mass spectrum (Figure 1a) is the protonated N-heterocyclic carbene ligand $H_2IMes\cdot H^+$ at m/z 307 (H_2IMes = 1,3-dimesityl-4,5-dihydroimidazol-2-ylidene). Furthermore, the ions $Cy_3P\cdot H^+$ at m/z 281 and $Cy_3PCH_3^+$ at m/z 295 were observed. The structure of the ion at m/z 295 was further confirmed by an MS/MS experiment (Figure S2b, Supporting Information). Mass spectrometric formation of these ions by in-source CID could be excluded, because the ESI-MS/MS spectrum for CID of the radical cation $\mathbf{2}^{\bullet+}$ at m/z 848 shows the peak at m/z 307 only with low intensity and fragment ions at m/z 281 and 295, respectively, were not observed (Figure 1b). Therefore, the free ligands PCy_3 and H_2IMes, most likely formed by dissociation of **2** and protonated by trace amounts of protic solvent, i.e. water, can be detected clearly from solution as protonated molecules. Interestingly, the MS/MS spectrum of $\mathbf{2}^{\bullet+}$ at m/z 848 showed the fragment ion $[Cy_3P{=}CHPh]^{\bullet+}$ at m/z 370, which was also observed for the MS/MS spectrum of $\mathbf{1}^{\bullet+},$[11] and the respective fragment ion $[H_2IMes{=}CHPh]^{\bullet+}$ at m/z 396. Comparable results were obtained studying Ru catalyst **3** (Figure S15).

Catalysts **4** and **5** are ether-tethered Ru alkylidene complexes, while catalyst **6** is a pyridine-tethered Ru alkylidene complex. The ESI mass spectra of these Ru catalysts dissolved in CH_2Cl_2 showed the corresponding radical cation $\mathbf{4}^{\bullet+}$ at m/z 600, $\mathbf{5}^{\bullet+}$ at m/z 626, and $\mathbf{6}^{\bullet+}$ at m/z 597 (Figure S17). Moreover, heterolysis of the Ru−Cl bond produced the cation $[\mathbf{5} - Cl]^+$ at m/z 591 by loss of Cl^- from **5** with low intensity. However, the ions $[\mathbf{4} - Cl]^+$ at m/z 565 and $[\mathbf{6} - Cl]^+$ at m/z 562 could not be clearly identified by their typical isotopic patterns in the ESI-MS spectra. The signals of the protonated ligand $Cy_3P\cdot H^+$ at m/z 281 and $H_2IMes\cdot H^+$ at m/z 307 are the base peaks in the ESI-MS spectra of **4** and of **5** and **6**, respectively. The ESI-MS/MS spectra of $\mathbf{4}^{\bullet+}$ at m/z 600, $\mathbf{5}^{\bullet+}$ at m/z 626, and $\mathbf{6}^{\bullet+}$ at

■ EXPERIMENTAL SECTION

General Remarks. CH_2Cl_2, CH_3OH, catalysts **2−6**, and alkali metal chlorides (LiCl, NaCl, KCl, and CsCl) were purchased form Aldrich (Steinheim, Germany) and used as received without further purification. All reactions and operations were performed at room temperature. Solvent CH_2Cl_2 was dried by distillation from CaH_2 as drying agent prior to use. Dry CH_3OH and CH_2Cl_2 were saturated with argon before use.

General Procedure for the Online Microreactor ESI-MS Study of the Alkali Metal Cationized Ru Complexes 2−6. A solution of 0.4 mg (5.5×10^{-5} M) of **2** in 10 mL of CH_2Cl_2 was prepared and mixed with a solution of 0.1 mg (2.4×10^{-4} M) of LiCl in 10 mL of CH_3OH using two respective syringes feeding a microreactor (Techlab, Peek mixing tee) coupled directly to the ESI-MS ion source. The flow rate of both solutions was set at 5 μL/min, allowing the study of the solution after a reaction time of approximately 12 s. The respective experiments of **2** with NaCl, KCl, and CsCl and of **3−6** with MCl (M = Li, Na, K, Cs) were performed analogously.

ESI-MS Experimental Conditions. The mass spectrometric measurements were performed on a Micromass Premier quadrupole time of flight (Q-Tof) instrument (Waters, Manchester) equipped with an ESI ion source containing a stainless steel metal spray capillary (127 μm inner diameter, 229 μm outer diameter, 181 mm length). A capillary voltage of 3.5 kV, source and desolvation temperatures of 50 °C, and a cone voltage of 20 V were applied as standard ESI operation conditions. Collision-induced dissociation (CID, collision gas argon with flow rate at 0.2 mL/min) was performed in the collision cell region; the collision energy was set to 2−30 eV for different ion species.

Note: the Ru complex ions gave their representative isotopic clusters in ESI MS spectra; the m/z values of these Ru complex ions as well as the MS/MS spectra shown in this paper are given for ^{102}Ru and ^{35}Cl.

Computational Details. We used the Gaussian 03 software package to perform density functional theory (DFT) calculations for the geometry optimizations of the ionic Ru species at the B3LYP level

m/z 597 (Figure S18) and their fragmentation pathways are shown in Schemes S1—S3.

2. ESI-MS Study of Ru Complexes 2—6 in the Presence of Alkali Metal Chlorides. We mixed 1 equiv of Ru catalyst **2**, dissolved in CH_2Cl_2, with 5 equiv of LiCl, dissolved in CH_3OH, using a microreactor directly coupled to the ESI source (Figure S1).[18] CH_3OH was used because of the solubility of alkali metal chlorides in this solvent. Here, the flow rate of both solutions was set at 5 μL/min, allowing the study of the solution after a reaction time of approximately 12 s. The ESI spectrum obtained (Figure S3a) revealed the formation of **2·Li$^+$** at m/z 855, which could be identified via the characteristic isotopic pattern (Figure S5). The highly increased relative intensity of cation $[2 - Cl]^+$ at m/z 813 in comparison to its CH_2Cl_2 solution (Figure 1a) may be due to the enhanced heterolysis of **2** induced by the added Lewis acid and the higher polarity of the solvent when mixing CH_2Cl_2 with CH_3OH.[11,12] In addition, the cationized dimer **2$_2$·Li$^+$** at m/z 1703 was detected with low intensity (Figure S9). The base peak was the protonated ligand ion $H_2IMes·H^+$ at m/z 307. The ion $Cy_3P·H^+$ at m/z 281 was also observed; however, it had lower intensity[11] (Figure S3a). Remarkably, the Li$^+$ cationized 14-electron Ru complex **2a·Li$^+$** at m/z 575, generated by dissociation of Cy_3P from **2·Li$^+$**, could be detected from solution with low intensity of $[2a·Li^+]/[2·Li^+]$ = 0.006, however unambiguously, as well as $[2a - Cl]^+$ at m/z 533 ($[2a - Cl]^+/[2a·Li^+]$ = 0.19). No signal of $[2 - H_2IMes]·Li^+$ at m/z 549 was observed. Comparable results have been obtained studying catalyst **3** in the presence of LiCl (Figures S15 and S16). The corresponding alkali metal adduct ions of catalyst **2** were obtained using NaCl, KCl, or CsCl (Figure S3), and the observed cationic Ru complexes of **2** are summarized in Scheme 2. These ions were further characterized

Scheme 2. Cationic Ru Carbene Species Detected in CH_3OH—CH_2Cl_2 Solution of Catalysts 2 in the Presence of Alkali Metal Chlorides
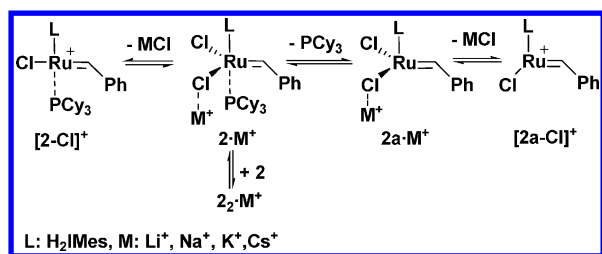
by MS/MS (Figure 2 and Figures S4, S13, and S14) and their isotopic patterns (Figures S5—S12) . The ratios of the intensities of $[2a·M^+]/[2·M^+]$, which can be compared quantitatively because of equal concentrations of **2** and of alkali chloride, respectively, in the same solvent mixture, are compiled in Table 1.

The ESI-MS/MS spectra of **2·M$^+$** (M = Li, Na, K, Cs; Figure 2) showed two main fragments: $[2 - Cl]^+$ at m/z 813 by loss of MCl and **2a·M$^+$** at m/z 575, 591, 607, and 701 by loss of PCy_3, respectively, when using a collision energy of ~10 eV (Figure 2). Interestingly, on going from Li$^+$ to Na$^+$ to K$^+$ and finally to Cs$^+$, the intensity ratio of the fragment ions $[2 - Cl]^+/[2a·M^+]$ decreased from 3.32 to 1.40 to 0.31 and finally to 0.24 (Table 2). The fragment ion Cs$^+$ was observed with low intensity, as shown for **2·Cs$^+$** (Figure 2d). However, no fragments $[2 - H_2IMes]·M^+$ were observed in the MS/MS of **2·M$^+$**. In contrast, $H_2IMes·H^+$ at m/z 307 was detected with low
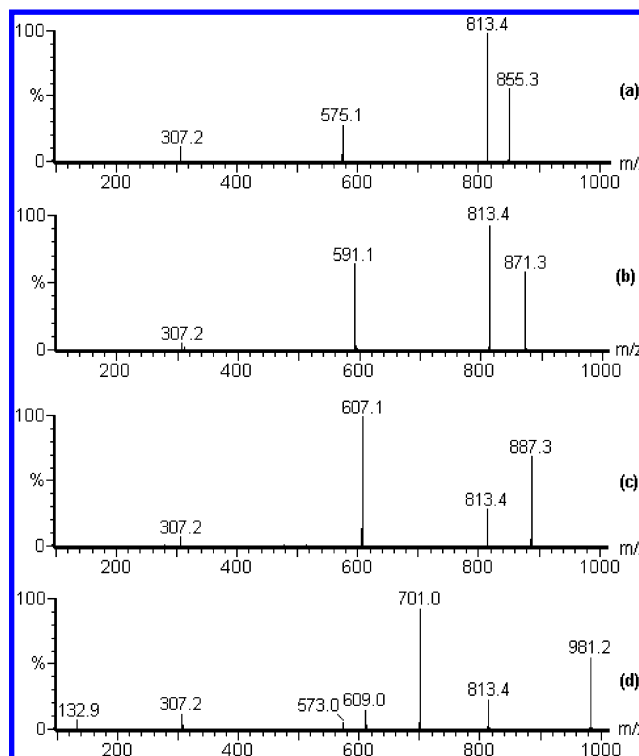
Figure 2. ESI-MS/MS spectra for CID of (a) **2·Li$^+$** at m/z 855, (b) **2·Na$^+$** at m/z 871, (c) **2·K$^+$** at m/z 887, and (d) **2·Cs$^+$** at m/z 981 (collision gas Ar; collision energy 10 eV).
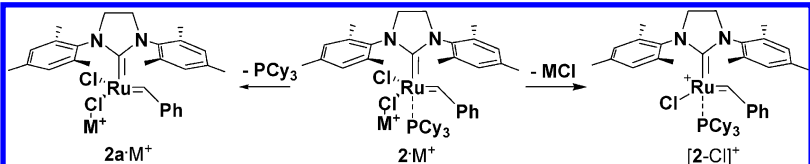
Table 1. ESI Spectra of Catalyst 2 in Solution in the Presence of Different Alkali Metal Salts: Ratios of the Intensities of the Signals of 2a·M$^+$ and 2·M$^+$

2@MCl[a]	2·M$^+$ (peak (m/z))	2a·M$^+$ (peak (m/z))	$I_{2a·M^+}/I_{2·M^+}$
2@LiCl	2·Li$^+$ (855)	2a·Li$^+$ (575)	0.006
2@NaCl	2·Na$^+$ (871)	2a·Na$^+$ (591)	0.04
2@KCl	2·K$^+$ (887)	2a·K$^+$ (607)	0.12
2@CsCl	2·Cs$^+$ (981)	2a·Cs$^+$ (701)	0.31

[a]A solution of **2** in CH_2Cl_2 was mixed with a CH_3OH solution of the alkali metal salt MCl.

intensity (Figure 2), whereas no fragment ion $Cy_3P·H^+$ at m/z 281 was formed. A smaller collision energy of ~6 eV was needed for the dissociation of **2a·M$^+$** in MS/MS (Figure S4). The main fragment ions of **2a·M$^+$** were formed by loss of the benzylidene ligand and are summarized in Table S1 and Scheme S4.

The corresponding alkali metal adduct ions (M = Li, K) of catalysts **4—6** could also be obtained by mixing the CH_2Cl_2 solution of the catalysts with the CH_3OH solution of MCl (Figures S19—S24). A collision energy of 12 eV was applied for CID of **4·Li$^+$—6·Li$^+$** (Figure S20) and 14 eV was used for **4·K$^+$—6·K$^+$** (Figure S22). The fragmentation pathways of **4·M$^+$** and of **5·M$^+$** are dominated by elimination of MCl/HCl and by loss of the (iPr-O)-benzylidene ligand. The MS/MS spectra of **4·M$^+$** showed fragmentation pathways very similar to those for the ion **1a·M$^+$**, the 14-electron complex of the first-generation Grubbs catalyst **1**.[12] Analogously, the MS/MS results of **5·M$^+$** were similar to those of **2a·M$^+$**. The MS/MS spectra of **6·M$^+$** showed the main fragment ion at m/z 526 by loss of MCl and HCl, as well as the protonated 4-allylpyridine at m/z 120 by dissociation of the alkylidene ligand.

Table 2. Main Dissociation Pathways of 2·M⁺ (M = Li, Na, K, Cs): Ratios of the Intensities of the Signals of [2 − Cl]⁺ and 2a·M⁺

M	2·M⁺ (peak (m/z))	2a·M⁺ (peak (m/z))	[2 − Cl]⁺ (peak (m/z))	$I_{[2\text{-}Cl]^+}/I_{2a\cdot M^+}{}^a$
Li	855	575	813	3.32
Na	871	591	813	1.40
K	887	607	813	0.31
Cs	981	701	813	0.24

[a]As given by the ratio of the intensities of the fragment ions [2 − Cl]⁺ and 2·M⁺ (Figure 2).
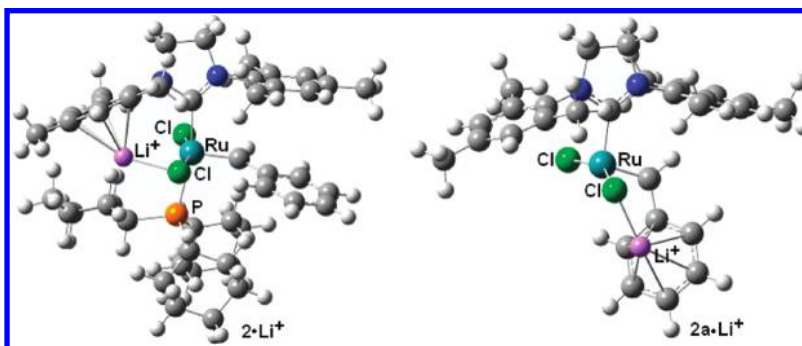
Figure 3. Optimized structures of 2·Li⁺ and 2a·Li⁺.

3. Computational Results. We performed DFT calculations of the structures and relative energies of Ru complexes **2**, **5**, and **6** with H₂IMes ligand. The comparison of the calculated optimized structures with the published structures from X-ray diffraction data of **2**,[13c] **5**,[14b] and **6**[15] shows a very good agreement (Tables S3, S5, and S6), taking into account that such calculations are known to overestimate by about 3% the metal−ligand bond distances.[16f]

Coordination of Li⁺ or K⁺ with 2 and 2a. Structural parameters of the optimized structures of **2**, **2·Li⁺**, and **2·K⁺** were summarized in Table S3 and of **2a**, **2a·Li⁺**, and **2a·K⁺** in Table S4. Figure 3 shows the calculated optimized structures of **2·Li⁺** and of **2a·Li⁺** in the gas phase. The respective potassium adducts are given in Figures S27 and S28. Li⁺ or K⁺, respectively, is coordinated to one chlorine atom of complex **2** as well as of **2a**. **2·M⁺** shows a Li−Cl distance of 2.28 Å and a K−Cl distance of 2.98 Å, and there is an elongation of the respective calculated Ru−Cl bonds from 2.50 Å in **2** to 2.60 Å in **2·Li⁺** and to 2.56 Å in **2·K⁺**. This Ru−Cl bond is found to be shortened to 2.41 Å in **2a**, to 2.51 Å in **2a·Li⁺** and to 2.46 Å in **2a·K⁺**. The changes in the Ru−Cl bond length indicate that coordination with Li⁺ weakens the Ru−Cl bond more than that with K⁺. That applies also to the respective structures of **5** and **6**. In **2a·M⁺** the M−C bond distances of the alkali metal cations to the benzene carbons of H₂IMes are calculated to be between 2.40 and 2.64 Å for Li⁺ and between 3.06 and 4.12 Å for K⁺, respectively, giving evidence for a π-cation interaction of M⁺ with an aromatic ring of the H₂IMes ligand (Table S7). Interestingly, the bond distances of the alkali metal cations of **2a·Li⁺** and **2a·K⁺** to the benzene carbon atoms of the benzylidene ligand of 2.42−2.61 Å in the case of Li⁺ and 3.28−3.60 Å in the case of K⁺, respectively, give also evidence for a π-cation interaction of M⁺ with the benzylidene ligand (Table S8).[19,20] The Ru−C(H₂IMes) bond is shortened from

2.05 Å in **2** to 1.94 Å in **2a**. In contrast, the Ru=C bond length of 1.86 Å is calculated to be the same in **2** and **2a**. Interestingly, cationization is calculated to have only a minor influence on the Ru−C(H₂IMes) bond distance, as well as on the Ru=C distance of the benzylidene ligand of **2** and **2a**, whereas the Ru−P distance of 2.54 Å in **2** is elongated to 2.57 Å in **2·Li⁺** and to 2.58 Å in **2·K⁺**.

The important energy changes by the ligand dissociation of PCy₃, chlorine, and H₂IMes, respectively, are summarized in Table 3, and further details of the computational results are

Table 3. Calculated Cationization and Important Bond Dissociation Energies of 2, 2·Li⁺, and 2·K⁺ (kcal mol⁻¹)

reaction channel	bare	M⁺ = Li⁺	M⁺ = K⁺
M⁺ + **2** → **2·M⁺**		−78.0	−37.8
2·M⁺ → **2a·M⁺** + PCy₃	19.6	32.7	22.4
2·M⁺ → [**2** − Cl]⁺ + MCl		31.6	37.7
2 → [**2** − Cl]⁺ + Cl⁻	121.3		
2 → [**2** − H₂IMes]⁺ + H₂IMes	49.2		

given in Table S2. The interaction energy of **2** is exothermic by 78.0 kcal mol⁻¹ with Li⁺ and 37.8 kcal mol⁻¹ with K⁺. The calculated Ru−PCy₃ dissociation energy of **2** of 19.6 kcal mol⁻¹ is in good agreement with previously calculated values of 14.4,[16a] 18.8,[16b] and 23.0 kcal·mol⁻¹,[16c] where different calculation methods were applied. The cationization increases the Ru−PCy₃ dissociation energy to 22.4 kcal mol⁻¹ for **2·K⁺** and to 32.7 kcal mol⁻¹ for **2·Li⁺**, respectively. The MCl dissociation energy of **2·Li⁺** is 31.6 kcal mol⁻¹ and of **2·K⁺** is 37.7 kcal mol⁻¹.
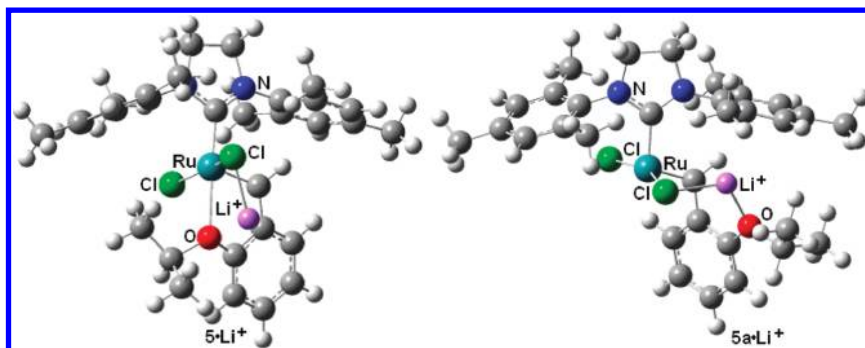
Figure 4. Optimized structures of **5·Li⁺** and **5a·Li⁺**.
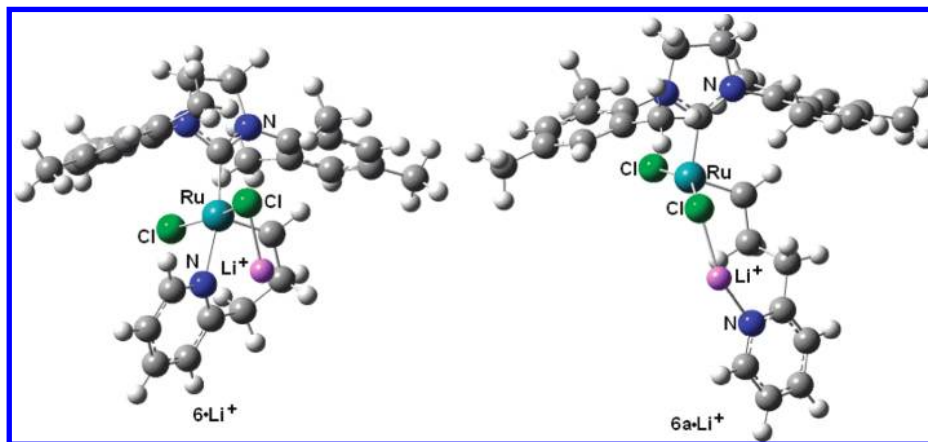
Figure 5. Optimized structures of **6·Li⁺** and **6a·Li⁺**.

Coordination of Li⁺ or K⁺ with 5, 5a, 6, and 6a. Structural parameters of the optimized structures of **5**, **5a**, **5·M⁺**, and **5a·M⁺** are summarized in Table S5. Li⁺ in **5·Li⁺** (Figure 4) and K⁺ in **5·K⁺** (Figure S31), respectively, are coordinated to one chlorine atom of complex **5**, showing a Li−Cl distance of 2.24 Å and a K−Cl distance of 3.04 Å (Table S5). The calculated Ru−Cl bond is elongated from 2.44 Å in **5** to 2.48 Å in **5·K⁺** and 2.53 Å in **5·Li⁺** (Table S5). In **5**, **5·Li⁺**, and **5·K⁺**, the length of the Ru−O bond was found to be 2.29, 2.46, and 2.30 Å, respectively. The O−Li⁺ distance in **5·Li⁺** of 1.96 Å and O−K⁺ distance in **5·K⁺** of 4.32 Å suggested strong coordination of Li⁺ and no coordination of K⁺ to the ether oxygen atom of the (*i*Pr-O)-benzylidene ligand.[20] In contrast, an additional π-cation interaction of K⁺ with C(2) and C(3) of an aromatic ring of the H₂IMes ligand, showing a distance of 3.28 Å, seems to be possible (Table S10).

Structural parameters of the optimized structures of **6**, **6a**, **6·M⁺**, and **6a·M⁺** are summarized in Table S6. The optimized structure of **6·Li⁺** (Figure 5) and of **6·K⁺** (Figure S35) shows a Li−Cl distance of 2.24 Å and a K−Cl distance of 2.97 Å. The calculated respective Ru−Cl bond is elongated from 2.49 Å in **6** to 2.52 Å in **6·K⁺** and 2.55 Å in **6·Li⁺**. The distance of the Ru-tethered N to Li⁺ in **6·Li⁺** is 2.13 Å, and the respective distance in **6·K⁺** is 3.16 Å. In **6**, **6·Li⁺**, and **6·K⁺**, the length of the Ru−N bond was found to be 2.14, 2.22, and 2.13 Å, respectively, which suggested that an strong coordination of Li⁺ to N might weaken the interaction of Ru to N, whereas K⁺ should have only a weak interaction with this N atom.

Just as for the Ru−PCy₃ dissociation step of **1** to **1a** or of **2** to **2a**, the alkoxy−Ru dissociation of **5** to **5a** and the alkylpyridine−Ru dissociation of **6** to **6a** via C−C bond

rotation gives the catalytically active 14-electron species in the catalytic cycle (Scheme 1). We also performed the calculations for **5a** and **6a**, as well as **5a·M⁺** and **6a·M⁺**, to reveal the cationization effect on the formation of the 14-electron species (Figures 4 and 5 and Tables S5 and S6). The Li−Cl distance in **5a·Li⁺** is 2.35 Å, and the K−Cl distance in **5a·K⁺** is 3.08 Å. The calculated Ru−Cl bond is elongated from 2.41 Å in **5a** to 2.46 Å in **5a·K⁺** and 2.48 Å in **5a·Li⁺**. In **5a**, **5a·Li⁺**, and **5a·K⁺**, the Ru−O distance was found to be 4.51, 4.08, and 4.61 Å, respectively, showing clearly no bonding between Ru and O. The distance of O−Li⁺ in **5a·Li⁺** is 1.94 Å, and the distance of O−K⁺ in **5a·K⁺** is 2.80 Å, suggesting additional coordination of Li⁺ as well as of K⁺ to the ether O atom of the benzylidene ligand.

Figure 5 shows the optimized structure of **6a·Li⁺** with a Li−Cl distance of 2.27 Å and **6a·K⁺** with a K−Cl distance of 3.03 Å and an elongation of the calculated respective Ru−Cl bond from 2.42 Å in **6a** to 2.47 Å in **6a·K⁺** and 2.51 Å in **6a·Li⁺** (Table S6). In **6a**, **6a·Li⁺**, and **6a·K⁺**, the Ru−N distance was found to be 5.93, 5.01, and 5.32 Å, respectively, showing clearly no bonding between Ru and N. The distance of N to Li⁺ in **6a·Li⁺** is 1.97 Å, and the respective distance in **6a·K⁺** is 2.80 Å, which suggested an additional coordination of Li⁺ as well as of K⁺ to the N atom. Remarkably, the Ru−C(H₂IMes) distance in **5** and **6** as well as in **5a** and **6a** is calculated to be practically not influenced by cationization. The same applies to the Ru═C distance of the benzylidene ligand (Tables S5 and S6).

The interaction energy of **5** and **6** with Li⁺ is calculated to be exothermic by 71.8 and 66.6 kcal mol⁻¹, respectively, and with K⁺ by 36.3 and 31.8 kcal mol⁻¹, respectively (Table 4). The relative energy between **5** and **5a** was calculated to be 13.8 kcal

Table 4. Calculated Cationization and Important Bond Dissociation Energies of 5, 6, 5·M⁺, and 6·M⁺

reaction channel	bare	$M^+ = Li^+$	$M^+ = K^+$
$M^+ + 5 \rightarrow 5 \cdot M^+$		−71.8	−36.3
$M^+ + 6 \rightarrow 6 \cdot M^+$		−66.6	−31.8
$M^+ + 5a \rightarrow 5a \cdot M^+$		−83.2	−40.0
$M^+ + 6a \rightarrow 6a \cdot M^+$		−85.9	−44.1
$5 \cdot M^+ \rightarrow 5a \cdot M^+$	13.8	2.4	11.4
$6 \cdot M^+ \rightarrow 6a \cdot M^+$	21.8	3.8	10.9

mol⁻¹ and is in good agreement with a previously calculated value of 10.8 kcal mol⁻¹ for a similar Ru−carbene complex.[21] Remarkably, it is reduced by cationization with K⁺ to 11.4 kcal mol⁻¹ and with Li⁺ to 2.4 kcal mol⁻¹. The relative energy between **6** and **6a** was calculated to be 21.8 kcal mol⁻¹, which is reduced by cationization with K⁺ to 10.9 kcal mol⁻¹ and with Li⁺ to 3.8 kcal mol⁻¹ (Table 4).

■ DISCUSSION

Under ESI conditions second-generation Grubbs catalysts **2** and **3** and Hoveyda−Grubbs catalysts **4** and **5**, as well as catalyst **6**, give the corresponding radical cation, just as for first-generation Ru catalysts **1**.[1,11] The protonated PCy₃ ligand at m/z 281 as well as the protonated N-heterocyclic carbene (NHC) ligand at m/z 307 can be directly detected in the mass spectrum, as well as [**M**-Cl]⁺ formed by loss of a chloride ligand (Figure 1). The MS/MS spectra of radical cation **2**^•⁺ and **3**^•⁺ give as base peak the fragment ion at m/z 370 formed by PCy₃ attacking the benzylidene moiety as already discussed for **1**^•⁺.[11] Therefore first and second generation as well as O- and N-tethered Ru catalysts can be characterized by ESI-MS with the isotopic patterns of the respective radical cations and by ESI-MS/MS. However, the radical cations are not catalytically active in the olefin metathesis reaction and are not suited for the study of the mechanism of the metathesis reactions. In contrast, first-generation catalyst **1** cationized with alkali metal ions is catalytically active and allows the study of the metathesis reactions in detail, in solution as well as in the gas phase.[12]

Our results clearly demonstrate that also Ru complexes **2**−**6** can be cationized in solution with alkali metal ions and that the cationized Ru species **2·M⁺**−**6·M⁺** can be detected using ESI-MS with high sensitivity. Most importantly, the catalytically active 14-electron Ru species **2a** and **3a** with NHC ligands are detectable directly from solution. The ratio [**2a·M⁺**]/[**2·M⁺**] (Table 1) was found to increase with decreasing Lewis acidity of M⁺ and was significantly higher than the respective ratio of first-generation catalyst **1**.[12] Thus, the concentration of **2a** in the dissociation equilibrium is enhanced by the NHC ligand of **2** in comparison to **1**, giving another clue to the higher catalytic activity of **2** compared to **1**.[22] This experimental result was confirmed by our DFT calculations (Table 3) showing that the Ru−P dissociation energy of **2** (19.6 kcal mol⁻¹) is lower than that of **1** (28.3 kcal mol⁻¹).[12]

DFT calculations and additionally the MS/MS results give evidence that the alkali-metal cation is coordinated to a chloride ligand of complex **2** (Figure 3). This is analogous to our results on first-generation catalyst **1**[12] and was observed as well for complexes **3**−**6**. Interestingly, the calculations of **2·Li⁺** and **2·K⁺** give evidence that the cation may be additionally coordinated to an aromatic ring of the H₂IMes ligand. This could explain

the enhanced coordination energy (Table 2) by about 10% compared to complex **1**.[12] As already discussed for complex **1**, the strong binding energy of **2** to Li⁺ (78 kcal mol⁻¹) or K⁺ (37.8 kcal mol⁻¹) had the effect that the CID gave informative fragmentations of the respective ions and not only loss of the alkali metal cation.

The ratio of the intensities [**2**-Cl]⁺/[**2a·M⁺**] decreased with decreasing Lewis acidity of M⁺ on going from Li⁺ to Na⁺ to K⁺ and to Cs⁺ (Figure 2 and Table 2). This is in accordance with the aforementioned effect of the Lewis acidity of M⁺ on the ratio [**2a·M⁺**]/[**2·M⁺**] in solution (Table 1) due to the decreasing Ru−PCy₃ and increasing Ru−Cl bond dissociation energy of **2·M⁺** on going from Li⁺ to Cs⁺ (Table 3). Thus, in MS/MS of **2·Li⁺** at m/z 865 (Figure 2a), the intensity of **2a·Li⁺** at m/z 575 was lower than that of [**2** − Cl]⁺ at m/z 813 due to the Ru−phosphine dissociation energy (32.7 kcal mol⁻¹) of **2·Li⁺** being higher than the Ru−Cl dissociation energy (31.6 kcal mol⁻¹) by 1.1 kcal mol⁻¹. However, in MS/MS of **2·K⁺** at m/z 887 (Figure 2c), the intensity of **2a·K⁺** at m/z 607 is higher than that of [**2** − Cl]⁺ at m/z 813 due to the Ru−phosphine dissociation energy of 22.4 kcal mol⁻¹ being 15 kcal mol⁻¹ lower than the Ru−Cl dissociation energy (37.7 kcal mol⁻¹) of **2·K⁺**. Interestingly, the influence of the Lewis acidity of M⁺ on the fragmentation ratio of the dissociation of PCy₃ and the elimination of MCl from **2·M⁺** of 1 order of magnitude (Table 2) is less than that observed for the respective fragmentations of **1·M⁺** of 2 orders of magnitude.[12] This observation gives also evidence that the stability of the neutral MCl fragment may be only a minor factor contributing to the observed fragmentation trend.

A significant effect of the Lewis acidity can also be observed on comparison of the MS/MS spectra of the 14-electron intermediates **2a·M⁺**. The ratio of the two main fragmentations of **2a·M⁺**, the elimination of the benzylidene ligand with HCl and of the benzylidene ligand alone, decreases with decreasing Lewis acidity on going from Li⁺ to Cs⁺ from 1.36 to 0.37 (Table S1 and Figure S4). In comparison to the fragmentation of **1a·M⁺** an enhanced elimination of the benzylidene ligand with HCl can be observed.[12]

The adduct ions of complexes **4**−**6** having a tethered benzylidene ligand showed interestingly the same Ru=C carbene scission reactions as were observed for the coordinatively unsaturated Ru complexes **1a** and **2a**, respectively. Thus, it can be concluded that the fragmentation of the adduct ions of complexes **4**−**6** occurs preferentially via the open, nontethered 14-electron species **4a**−**6a**. The scission of the Ru=C bond with carbene ligand is an important dissociation pathway of the 14-electron Ru complexes,[23] and the following dehydrogenation phenomena[24] also have been widely observed in MS/MS spectra of other organic phosphine−metal complexes via a C−H activation mechanism,[25] which could rationalize the formation of the fragment ion at m/z 305 in ESI-MS/MS of **2a·M⁺** (Figure S4) due to H transfer from the H₂IMes to the benzylidene ligand catalyzed by agostic interaction[26] of a coordinately unsaturated transition metal with the C−H bond of the H₂IMes ligand. Similar agostic interactions were reported in ruthenium complexes.[27]

Most interestingly, our calculations gave evidence that cationization of Hoveyda−Grubbs catalyst **5** and pyridine-tethered catalyst **6** could increase the concentration of catalytically active 14-electron species **5a·M⁺** and **6a·M⁺**, respectively, because M⁺ seems to coordinate not only to Cl but also to O or N of the tethered ligand, which decreased the

bond dissociation energy of the Ru−O and Ru−N bonds, respectively. Thus, cationization with alkali metal cations could possibly enhance the catalytic activity of catalysts **5** and **6** with increasing Lewis acidity of the alkali metal cation. In contrast, it was shown that the catalytic activity of first-generation Grubbs catalysts, such as **1**, decreased with increasing acidity of the alkali metal cation.[12] The respective effect should be expected for second-generation catalysts such as **2**.

CONCLUSIONS

The alkali metal cationizations of Ru−carbene catalysts **2−6** were developed in analogy to **1** as a promising general strategy for ESI-MS studies of second-generation Grubbs and of Hoveyda−Grubbs catalysts. Most importantly, in solutions of Ru complexes **2** and **3** the 14-electron Ru species **2a** and **3a**, respectively, could be detected as their M+ adduct ions directly by ESI-MS. The relative equilibrium concentration of the 14-electron complex, which is generally assumed to be the catalytically active species, was found to be much higher than in solutions of first-generation catalyst **1**. CID of the cationized catalysts **2−6** allowed a detailed fragmentation study. These experimental results were compared with the results of DFT calculations of bare and cationized **2**, **5**, and **6** as well as of the respective 14-electron species **2a**, **5a**, and **6a**. Whereas the equilibrium concentration of the 14-electron species of second-generation Grubbs catalyst **2** was shown to decrease by cationization and, however, to increase with decreasing Lewis acidity of the cation, DFT calculations gave evidence that the equilibrium concentration of the 14-electron species will be enhanced in the case of Hoveyda−Grubbs catalyst **5** and also in the case of the pyridine-tethered catalyst **6**. Our results may be helpful for optimizing the application of second-generation Grubbs and Hoveyda−Grubbs catalysts in olefin metathesis reactions.

ASSOCIATED CONTENT

Ⓢ Supporting Information

Figures and tables giving additional ESI-MS/MS spectra, optimized structures, and the proposed fragmentation pathways of ions studied in this paper. This material is available free of charge via the Internet at http://pubs.acs.org.

AUTHOR INFORMATION

Corresponding Author
*Tel: 49/441/7983718. Fax: 49/441/798193718. E-mail: Juergen.Metzger@uni-oldenburg.de.

Notes
The authors declare no competing financial interest.

ACKNOWLEDGMENTS

REFERENCES

(1) Van Berkel, G. J. In *Electrospray Ionization Mass Spectrometry: Fundamentals, Instrumentation and Applications*; Cole, R. B., Ed.; Wiley: New York, 1997; pp 65−105.

(2) Kebarle, P.; Verkerk, U. H. *Mass Spectrom. Rev.* **2009**, *28*, 898.

(3) (a) Colton, R.; D'Agostino, A.; Traeger, J. C. *Mass Spectrom. Rev.* **1995**, *14*, 79. (b) Traeger, J. C. *Int. J. Mass Spectrom.* **2000**, *200*, 387.

(4) Chen, P. *Angew. Chem., Int. Ed.* **2003**, *42*, 2832.

(5) (a) Markert, C.; Pfaltz, A. *Angew. Chem., Int. Ed.* **2004**, *43*, 2498. (b) Muller, C. A.; Pfaltz, A. *Angew. Chem., Int. Ed.* **2008**, *47*, 3363. (c) Teichert, A.; Pfaltz, A. *Angew. Chem., Int. Ed.* **2008**, *47*, 3360.

(6) (a) Santos, L. S.; Knaack, L.; Metzger, J. O. *Int. J. Mass Spectrom.* **2005**, *246*, 84. (b) Eberlin, M. N. *Eur. J. Mass Spectrom.* **2007**, *13*, 19. (c) Santos, L. S. *Eur. J. Org. Chem.* **2008**, 235.

(7) (a) Sabino, A. A.; Machado, A. H. L.; Correia, C. R. D.; Eberlin, M. N. *Angew. Chem., Int. Ed.* **2004**, *43*, 2514. (b) Santos, L. S.; Pavam, C. H.; Almeida, W. P.; Coelho, F.; Eberlin, M. N. *Angew. Chem., Int. Ed.* **2004**, *43*, 4330. (c) Zhang, X.; Liao, Y.; Qian, R.; Wang, H.; Guo, Y. *Org. Lett.* **2005**, *7*, 3877. (d) Santos, L. S.; Rosso, G. B.; Pilli, R. A.; Eberlin, M. N. *J. Org. Chem.* **2007**, *72*, 5809. (e) Comelles, J.; Pericas, A.; Moreno-Mañas, M.; Vallribera, A.; Drudis-Solé, G.; Lledos, A.; Parella, T.; Roglans, A.; García-Granda, S.; Roces-Fernández, L. *J. Org. Chem.* **2007**, *72*, 2077. (f) Roithová, J.; Schröder, D. *Chem. Eur. J.* **2008**, *14*, 2180. (g) Santos, L. S.; Metzger, J. O. *Rapid Commun. Mass Spectrom.* **2008**, *22*, 898. (h) Santos, L. S.; Metzger, J. O. *Angew. Chem., Int. Ed.* **2006**, *45*, 977.

(8) Grubbs, R. H., Ed. *Handbook of Metathesis*; Wiley-VCH: Weinheim, Germany, 2003; Vols. *1−3*.

(9) Reviews for metathesis reactions: (a) Grubbs, R. H.; Chang, S. *Tetrahedron* **1998**, *54*, 4413. (b) Trnka, T. M.; Grubbs, R. H. *Acc. Chem. Res.* **2001**, *34*, 18. (c) Grubbs, R. H. *Tetrahedron* **2004**, *60*, 7117. (d) Fürstner, A. *Angew. Chem., Int. Ed.* **2000**, *39*, 3012.

(10) (a) Hinderling, C.; Adlhart, C.; Chen, P. *Angew. Chem., Int. Ed.* **1998**, *37*, 2685. (b) Adlhart, C.; Hinderling, C.; Baumann, H.; Chen, P. *J. Am. Chem. Soc.* **2000**, *122*, 8204.

(11) Wang, H.-Y.; Metzger, J. O. *Organometallics* **2008**, *27*, 2761.

(12) Wang, H.-Y.; Yim, W.-L.; Klüner, T.; Metzger, J. O. *Chem. Eur. J.* **2009**, *15*, 10948.

(13) (a) Scholl, M.; Trnka, T. M.; Morgan, J. P.; Grubbs, R. H. *Tetrahedron Lett.* **1999**, *40*, 2247. (b) Scholl, M.; Ding, S.; Lee, C. W.; Grubbs, R. H. *Org. Lett.* **1999**, *1*, 953. (c) Love, J. A.; Sanford, M. S.; Day, M. W.; Grubbs, R. H. *J. Am. Chem. Soc.* **2003**, *125*, 10103.

(14) (a) Kingsbury, J. S.; Harrity, J. P. A; Bonitatebus, P. J. Jr.; Hoveyda, A. H. *J. Am. Chem. Soc.* **1999**, *121*, 791. (b) Garber, S. B.; Kingsbury, J. S.; Gray, B. L.; Hoveyda, A. H. *J. Am. Chem. Soc.* **2000**, *122*, 8168.

(15) Ung, T.; Hejl, A.; Grubbs, R. H.; Schrodi, Y. *Organometallics* **2004**, *23*, 5399.

(16) (a) Fomine, S.; Tlenkopatchev, M. A. *Organometallics* **2007**, *26*, 4491. (b) Zhao, Y.; Truhlar, D. G. *Org. Lett.* **2007**, *9*, 1967. (c) Cavallo, L. *J. Am. Chem. Soc.* **2002**, *124*, 8965. (d) Tsipis, A. C.; Orpen, A. G.; Harvey, J. N. *Dalton Trans.* **2005**, 2849. (e) Adlhart, C.; Chen, P. In *Handbook of Metathesis*; Grubbs, R. H., Ed.; Wiley-VCH: Weinheim, Germany, 2003; Vol. *1*, pp 132−172. (f) Gatard, S.; Kahlal, S.; Méry, D.; Nlate, S.; Cloutet, E.; Saillard, J.-Y.; Astruc, D. *Organometallics* **2004**, *23*, 1313.

(17) Frisch, M. J.; Trucks, G. W.; Schlegel, H. B.; Scuseria, G. E.; Robb, M. A.; Cheeseman, J. R; J. A. Montgomery, J.; Vreven, T.; Kudin, K. N.; Burant, J. C.; Millam, J. M.; Iyengar, S. S.; Tomasi, J.; Barone, V.; Mennucci, B.; Cossi, M.; Scalmani, G.; Rega, N.; Petersson, G. A.; Nakatsuji, H.; Hada, M.; Ehara, M.; Toyota, K.; Fukuda, R.; Hasegawa, J.; Ishida, M.; Nakajima, T.; Honda, Y.; Kitao, O.; Nakai, H.; Klene, M.; Li, X.; Knox, J. E.; Hratchian, H. P.; Cross, J. B.; Adamo, C.; Jaramillo, J.; Gomperts, R.; Stratmann, R. E.; Yazyev, O.; Austin, A. J.; Cammi, R.; Pomelli, C.; Ochterski, J. W.; Ayala, P. Y.; Morokuma, K.; Voth, G. A.; Salvador, P.; Dannenberg, J. J.; Zakrzewski, V. G.; Dapprich, S.; Daniels, A. D.; Strain, M. C.; Farkas, O.; Malick, D. K.; Rabuck, A. D.; Raghavachari, K.; Foresman, J. B.; Ortiz, J. V.; Cui, Q.; Baboul, A. G.; Clifford, S.; Cioslowski, J.; Stefanov, B. B.; Liu, G.; Liashenko, A.; Piskorz, P.; Komaromi, I.; Martin, R. L.; Fox, D. J.; Keith, T.; Al-Laham, M. A.; Peng, C. Y.; Nanayakkara, A.; Challacombe, M.; Gill, P. M. W.; Johnson, B.; Chen, W.; Wong, M. W.; Gonzalez, C.; Pople, J. A. *Gaussian 03, Revision D.01*; Gaussian, Inc., Wallingford, CT, 2004.

(18) (a) Meyer, S.; Metzger, J. O. *Anal. Bioanal. Chem.* **2003**, *377*, 1108. (b) Fürmeier, S.; Metzger, J. O. *J. Am. Chem. Soc.* **2004**, *126*, 14485. (c) Marquez, C. A.; Metzger, J. O. *Chem. Commun.* **2006**, *14*, 1539. (d) Marquez, C. A.; Fabbretti, F.; Metzger, J. O. *Angew. Chem., Int. Ed.* **2007**, *46*, 6915.

(19) (a) Ma, J. C.; Dougherty, D. A. *Chem. Rev.* **1997**, *97*, 1303. (b) Amicangelo, J. C.; Armentrout, P. B. *J. Phys. Chem. A* **2000**, *104*, 11420.

(20) (a) Hu, J.; Barbour, L. J.; Gokel, G. W. *J. Am. Chem. Soc.* **2002**, *124*, 10940. (b) Gokel, G. W.; Barbour, L J.; Ferdani, R.; Hu, J. *Acc. Chem. Res.* **2002**, *35*, 878. (c) Schmitt, W.; Anson, C. E.; Hill, J. P.; Powell, A. K. *J. Am. Chem. Soc.* **2003**, *125*, 11142. (d) Mecozzi, S.; West, A. P. Jr.; Dougherty, D. A. *J. Am. Chem. Soc.* **1996**, *118*, 2307.

(21) Solans-Monfort, X.; Pleixats, R.; Sodupe, M. *Chem. Eur. J.* **2010**, *16*, 7331.

(22) Sanford, M. S.; Love, J. A.; Grubbs, R. H. *J. Am. Chem. Soc.* **2001**, *123*, 6543.

(23) Torker, S.; Merki, D.; Chen, P. *J. Am. Chem. Soc.* **2008**, *130*, 4808.

(24) (a) Feichtinger, D.; Plattner, D. A.; Chen, P. *J. Am. Chem. Soc.* **1998**, *120*, 7125. (b) Richardson, D. E.; Alameddin, N. G.; Ryan, M. F.; Hayes, T.; Eyler, J. R.; Siedle, A. R. *J. Am. Chem. Soc.* **1996**, *118*, 11244.

(25) (a) Labinger, J. A.; Bercaw, J. E. *Nature* **2002**, *417*, 507. (b) Courchay, F. C.; Sworen, J. C.; Ghiviriga, I.; Abboud, K. A.; Wagener, K. B. *Organometallics* **2006**, *25*, 6074.

(26) Brookhart, M.; Green, M. L. H.; Parkin, G. *Proc. Natl. Acad. Sci. U.S.A.* **2007**, *104*, 6908.

(27) (a) Matsubara, T.; Koga, N.; Musaev, D. G.; Morokuma, K. *J. Am. Chem. Soc.* **1998**, *120*, 12692. (b) Matsubara, T.; Koga, N.; Musaev, D. G.; Morokuma, K. *Organometallics* **2000**, *19*, 2318. (c) Mathew, J.; Koga, N.; Suresh, C. H. *Organometallics* **2008**, *27*, 4666.